journal

J. Am. Ceram. Soc., 79 [7] 1801–809 (1996)

Grain Boundary Mobility in Y_2O_3: Defect Mechanism and Dopant Effects

Pei-Lin Chen* and I-Wei Chen*

Department of Materials Sciences and Engineering, University of Michigan, Ann Arbor, Michigan 48109-2136

The effects of the dopants, Mg^{2+}, Sr^{2+}, Sc^{3+}, Yb^{3+}, Gd^{3+}, La^{3+}, Ti^{4+}, Zr^{4+}, Ce^{4+}, and Nb^{5+}, on the grain boundary mobility of dense Y_2O_3 have been investigated from 1500° to 1650°C. Parabolic grain growth has been observed in all cases over a grain size from 0.31 to 12.5 μm. Together with atmospheric effects, the results suggest that interstitial transport is the rate-limiting step for diffusive processes in Y_2O_3, which is also the case in CeO_2. The effect of solute drag cannot be ascertained but the anomalous effect of undersized dopants (Ti and Nb) on diffusion enhancement, previously reported in CeO_2, is again confirmed. Indications of very large binding energies between aliovalent dopants and oxygen defects are also observed. Overall, the most effective grain growth inhibitor is Zr^{4+}, while the most potent grain growth promoter is Sr^{2+}, both at 1.0% concentration.

I. Introduction

Our recent experimental studies of grain boundary mobility in CeO_2,[1,2] a fluorite-structured oxide, have revealed several important features. First, grain boundary mobility is controlled by cation diffusivity, and cations diffuse by an interstitial mechanism that can be enhanced by the presence of oxygen vacancies. Second, at high dopant concentrations, a solute drag mechanism operates that can suppress grain boundary mobility. Third, grain boundary mobility is influenced by dopant–defect interaction which is charge and size dependent. Fourth, severely undersized dopants have a tendency to markedly enhance grain boundary mobility, probably due to the distortion of the surrounding lattice that apparently facilitates defect migration. These new results are consistent with other reports on the structure, energetics, and kinetics of the CeO_2 system. In fact, a review of the previous data in the literature suggests that the cation interstitial mechanism may be general for hypostoichiometric fluorite-structured oxides (AO_{2-x}). For example, self-diffusivity of U has been reported to increase with x at $x > 0.02$ in UO_{2-x}.[3] Likewise, creep and evaporation studies in $U_{1-y}Pu_yO_{2-x}$[4–6] and grain growth studies in $U_{1-y}Ca_yO_{2-x}$[7] both witnessed enhanced kinetics with increasing x. These observations are consistent with a cation interstitial mechanism which may be justified by the availability of large, unoccupied interstitial sites in the fluorite structure.[1,2]

Y_2O_3 has a C-type rare-earth oxide crystal structure. As shown in Fig. 1, this structure may be pictured as a modified fluorite-type cubic structure with one fourth of the anion sites vacant and regularly arranged. Like fluorite-structured oxides, oxygen vacancies and interstitials are the major defects in pure yttrium oxide.[8–11] Also like fluorite-structured oxides, Y_2O_3 can dissolve a large amount of aliovalent cations. This is accompanied by creating charge-compensating oxygen vacancies when acceptor dopants are present,[12] and oxygen interstitials when donor dopants are present.[13,14] These anion defects facilitate oxygen diffusion. Indeed, it is known[15,16] that oxygen anion diffusion is much faster than yttrium cation diffusion in pure Y_2O_3. Thus, cation diffusion is the rate-controlling step for grain boundary migration at all compositions. Since cation doping can be readily conducted within the solubility limit, Y_2O_3, like CeO_2, is a good candidate for investigating cation dopant effects on grain boundary mobility. The cubic symmetry of this oxide further assures a lack of strong anisotropy in grain boundary mobility which could otherwise complicate grain growth behavior.

In order to understand the effects of dopants on mobility, oversized and undersized dopants of both donor and acceptor types are investigated here. They include, in the order of increasing charge and size, Mg^{2+}, Sr^{2+}, Sc^{3+}, Yb^{3+}, Gd^{3+}, La^{3+}, Ti^{4+}, Zr^{4+}, Ce^{4+}, and Nb^{5+}, all of which have also been investigated in our grain growth study of CeO_2.[2] Since Y^{3+} and Ce^{4+} have very similar ionic radii for both 6-fold (as in C-type structure) and 8-fold (as in fluorite structure) coordination,[17] a direct comparison of the dopant behavior in these two closely related oxide structures is possible. Table I summarizes the literature data of ionic radius, solubility, and Vegard's slope (on the basis of cation percent) of these dopants.

II. Theoretical Considerations

Following the analysis of defect chemistry for CeO_2 in our previous paper,[1,2] we estimate the defect concentration in Y_2O_3 in the following way. Starting with

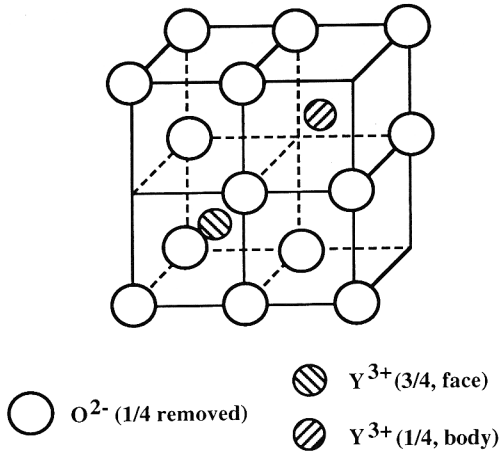

Fig. 1. Crystal structure of Y_2O_3. Three quarters of cations are in cubes in which the missing oxygens are along a face diagonal. One quarter of cations are in cubes in which the missing oxygens are along a body diagonal.

C. A. Handwerker—contributing editor

Manuscript No. 192269. Received October 9, 1995; approved February 1, 1996.
Presented at the 96th Annual Meeting of the American Ceramic Society, Cincinnati, OH, April 26, 1994 (Synthesis, Processing, and Microstructure Symposium, Paper No. SXVIIc-126-94).
Supported by the U.S. Department of Energy under Grant No. DE-FG02-87ER-45302.
*Member, American Ceramic Society.

Table I. Ionic Radius, Vegard's Slope, and Solubility of MO_x in Y_2O_3

	Ionic radius (Å)†	Vegard's slope‡	Solubility ($\%MO_x$)	References
Mg^{2+}	0.72		1 (1700°C)	18
Sr^{2+}	1.18	0.0989	1 (1700°C)	12, 19
Sc^{3+}	0.745		100	20
Yb^{3+}	0.868			
Y^{3+}	0.9			
Gd^{3+}	0.938		70 (1600°C)	21
La^{3+}	1.032		16 (1400°C)	22
Ti^{4+}	0.605			
Zr^{4+}	0.72	−0.0883	10 (1400°C)	23
Ce^{4+}	0.87	0.1085	28 (1600°C)	14
Nb^{5+}	0.64	−0.0011	30 (1500°C)	24

†Reference 17. All for 6-fold coordination. ‡$\Delta V/V_O = \alpha C$ (α = Vegard's slope, C = solute atomic fraction, V_O = unit-cell volume of pure Y_2O_3).

Schottky defect for cation:

$$\text{null} \xleftrightarrow{\Delta G_S} 2V_Y''' + 3V_O^{\cdot\cdot} \tag{1}$$

Frenkel defect for cation:

$$Y_Y \xleftrightarrow{\Delta G_F} V_Y''' + Y_i^{\cdot\cdot\cdot} \tag{2}$$

Frenkel defect for anion:

$$O_O \xleftrightarrow{\Delta G_F^A} O_i'' + V_O^{\cdot\cdot} \tag{3}$$

we obtain

$$[V_Y'''] = [V_O^{\cdot\cdot}]^{-1.5} K_S^{0.5} \exp\left[-\frac{\Delta G_S/2}{kT}\right] \tag{4}$$

$$= [O_i'']^{1.5}\left(\frac{K_S^{0.5}}{K_F^{A\,1.5}}\right)\exp\left[-\frac{\Delta G_S/2 - 3\Delta G_F^A/2}{kT}\right] \tag{5}$$

$$[Y_i^{\cdot\cdot\cdot}] = [V_O^{\cdot\cdot}]^{1.5}\left(\frac{K_F}{K_S^{0.5}}\right)\exp\left[-\frac{\Delta G_F - \Delta G_S/2}{kT}\right] \tag{6}$$

$$= [O_i'']^{-1.5}\left(\frac{K_F K_F^{A\,1.5}}{K_S^{0.5}}\right) \times \exp\left[-\frac{\Delta G_F - \Delta G_S/2 + 3\Delta G_F^A/2}{kT}\right] \tag{7}$$

In the above, K_F, K_S, and K_F^A are the preexponential, temperature-independent, factors of the reaction constants of (1), (2), and (3), respectively. Cation diffusivity, which is proportional to the cation defect concentration, is thus strongly dependent on the concentration of oxygen defects.

In pure Y_2O_3, oxygen defect concentrations are determined by the following reactions:

Oxidation (p-type):

$$\tfrac{1}{2}O_2 \xleftrightarrow{\Delta H_{O_2}^{(O)}} O_i'' + 2h^{\cdot} \tag{8}$$

Reduction (n-type):

$$O_O \xleftrightarrow{\Delta H_{O_2}^{(R)}} V_O^{\cdot\cdot} + 2e' + \tfrac{1}{2}O_2 \tag{9}$$

Along with the reaction of anion Frenkel defects (Eq. (3)), we obtain

p-type:

$$[V_O^{\cdot\cdot}] = \frac{K_F^A}{K_{O_2}^{(O)1/3}}\exp\left[-\frac{\Delta G_F^A - \Delta H_{O_2}^{(O)}/3}{kT}\right] \propto P_{O_2}^{-1/6} \tag{10}$$

$$[O_i''] = K_{O_2}^{(O)1/3}\exp\left[-\frac{\Delta H_{O_2}^{(O)}/3}{kT}\right] \propto P_{O_2}^{1/6} \tag{11}$$

n-type:

$$[V_O^{\cdot\cdot}] = K_{O_2}^{(R)1/3}\exp\left[-\frac{\Delta H_{O_2}^{(R)}/3}{kT}\right] \propto P_{O_2}^{-1/6} \tag{12}$$

$$[O_i''] = \frac{K_F^A}{K_{O_2}^{(R)1/3}}\exp\left[-\frac{\Delta G_F^A - \Delta H_{O_2}^{(R)}/3}{kT}\right] \propto P_{O_2}^{1/6} \tag{13}$$

In the above, $K_{O_2}^{(O)}$ and $K_{O_2}^{(R)}$ are the preexponential, temperature-independent but pressure-dependent, factors of reaction constants of (8) and (9), respectively. According to Tallen and Vest,[25] Y_2O_3 exhibits p-type conduction at low temperature and high oxygen pressure, and n-type conduction at high temperature and low oxygen pressure. This n–p boundary is shown in Fig. 2(a) to guide our analysis. Our experiments on undoped Y_2O_3 were conducted mostly in air at temperatures not exceeding 1650°C; we therefore expect p-type behavior. This information on conductivity also allows us to approximately estimate the concentration of intrinsic defects, $[O_i'']$ in the case of p-type and $[V_O^{\cdot\cdot}]$ in the case of n-type, by assuming a reasonable value for the mobility of electrons and holes ($\mu_e = \mu_h = 10^{-2}$ cm^2/(V·s)). The calculated results are shown in Fig. 2(b) as a function of oxygen partial pressures. It is clear from Fig. 2(b) that under our experimental conditions, the concentration of intrinsic defects is very low indeed and it would be rather unrealistic to attempt to control the dopant concentration to comparably low values. Therefore, unlike in our CeO_2 study, we have not studied the dopant effect in the intrinsic regime but instead limited ourselves to the extrinsic regime in large part.

In the extrinsic regime, every two divalent acceptors create one $V_O^{\cdot\cdot}$. This increases $[Y_i^{\cdot\cdot\cdot}]$ but decreases $[V_Y''']$. Conversely, every two tetravalent donors create one O_i'', so that $[V_Y''']$ is increased but $[Y_i^{\cdot\cdot\cdot}]$ is decreased. Since grain boundary mobility is directly proportional to cation diffusivity regardless of whether it is grain boundary or lattice diffusion (solute drag) controlled, grain growth studies under different atmospheres together with different dopants in the extrinsic regime allow us to indirectly determine the diffusion mechanism in Y_2O_3. These findings can then be compared with those in CeO_2.

III. Experimental Procedure

Monosized spherical yttria powders were first prepared following a homogeneous precipitation method which was similar to the one used by Sordelet and Akinc.[26] Yttrium nitrate ($Y(NO_3)_3$, Alfa) and urea ($(NH_2)_2CO$, Fisher) were used as starting materials. After being calcined at 700°C in air for 1.5 h, the obtained yttria powders, with a particle size of 0.23 μm, were dispersed in isopropyl alcohol to which a desired amount of dissolved dopant nitrate was added. (Dopant concentrations were fixed at 1.0% of the total cations. This is the same amount used in the CeO_2 study in the extrinsic regime.) The slurry was poured through a 20 μm nylon screen and dried under heat while being stirred. The dried powders were sifted through a

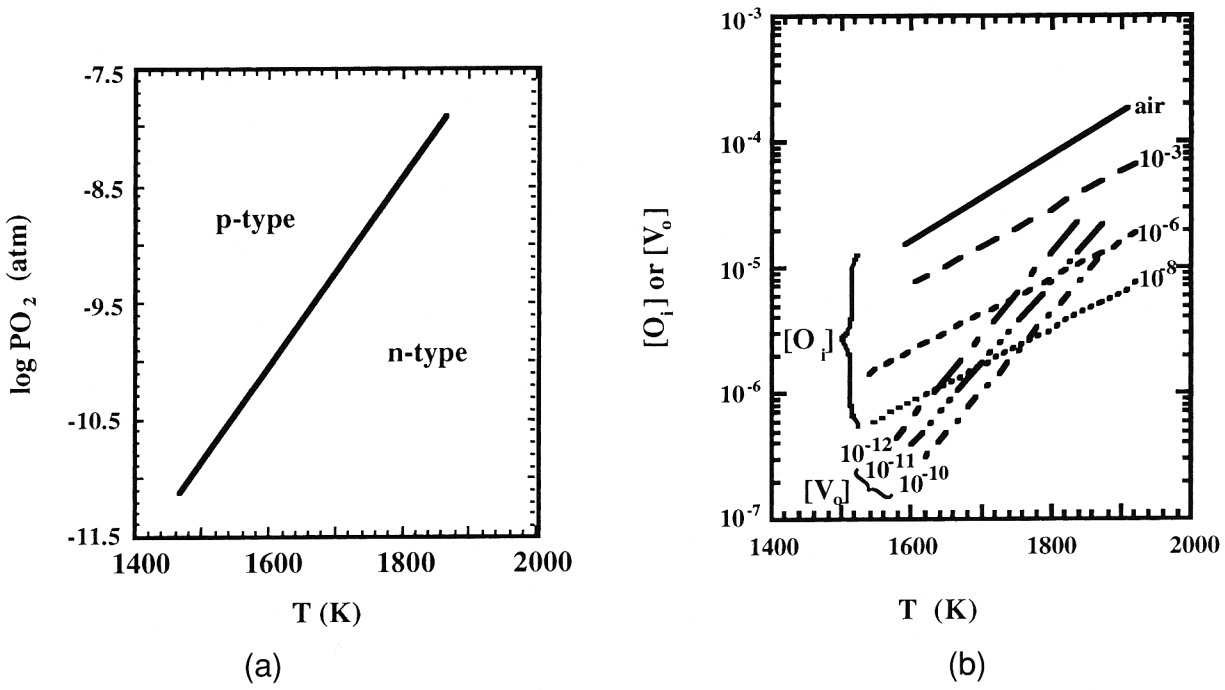

Fig. 2. (a) Boundary of *n*-type and *p*-type conduction in Y_2O_3. (b) Estimated concentration of intrinsic anion defects in Y_2O_3.

100 μm nylon screen and recalcined. Throughout the above process, plastic ware was used to avoid silica contamination.

The calcined powders were dry-pressed into pellets with a diameter of 10 mm and further isostatically pressed at 310 MPa. The green density after isostatic pressing was about 43% of the theoretical density. For sintering, a constant heating rate, 10°C/min, was chosen to reach the desired temperatures ranging from 1500° to 1650°C. Samples were held there from 1 to 63 h, and furnace cooled. To minimize silica contamination, firing in air was conducted using a dedicated "clean" furnace. Flowing gas of 2% H_2 in Ar was also used in a tube furnace when a reducing atmosphere was needed.

The microstructures of the sintered specimens were characterized by a scanning electron microscope (SEM) after polishing and thermal etching. The grain size was obtained for samples with a density higher than 99% by multiplying the average linear intercept length of at least 500 grains by 1.56.[27]

IV. Results

(1) *Microstructure*

Figure 3 shows selected microstructures to demonstrate the difference in grain size. Among all the dopants, Zr-doped Y_2O_3 has the smallest grain size, while Sr-doped Y_2O_3 has the largest one, under the same sintering conditions. As shown in Figs. 3(b) and (d), the grain size of Sr-doped Y_2O_3 is more than 10 times that of Zr-doped Y_2O_3. Abnormal grain growth seems absent in these microstructures. To ascertain this, grain size distributions were measured and plotted in a normalized form in Fig. 4. They appear to follow each other closely, centering around the mean grain size, despite the large difference in the average grain size. Thus, a time-invariant grain size distribution has been attained in our experiments. It also justifies our use of the mean grain size to characterize grain growth kinetics.

(2) *Grain Boundary Mobility*

Following the procedure established in our previous papers,[1,2] we found that the mobility data agree with the parabolic law well:

$$d^2 - d_0^2 = 2M\gamma(t - t_0) \tag{14}$$

In the above d_0 is the reference grain size at time t_0, d is the average grain size at time t, and γ is the grain boundary energy. To avoid the effect of porosity on grain growth, t_0 was appropriately chosen so that porosity was less than 1%. Typically, it lies between 3 h at 1500°C and 1 h at 1650°C. If the mobility and grain boundary energy are not a function of time (or grain size), then Eq. (14) predicts a straight line relation between $d^2 - d_0^2$ and $t - t_0$. This relation is demonstrated in Fig. 5, from which the slope can be computed to obtain $2M\gamma$. Since the value of the slope varies over several orders of magnitude, it most likely reflects the large influence of the dopants on grain boundary mobilities. (Grain boundary energy typically varies by no more than a factor of 2 or 3 only.) In view of this, we have used $\gamma = 0.3$ J/m^2 in our previous work to obtain an estimate of the mobility. The same practice is also adopted here. The mobilities evaluated in this way are tabulated in Table II for future reference. These data are anlayzed in the following to elucidate the diffusion and grain growth mechanisms.

V. Cation Interstitial Mechanism

(1) *Undoped Y_2O_3*

The grain boundary mobility of pure Y_2O_3 is higher in reduced atmosphere than in air. These data are shown in Fig. 6 and clearly indicate cation diffusion is via the cation interstitial mechanism. In the intrinsic regime, the temperature dependence of $[Y_i^{\cdots}]$ can be analyzed by combining Eqs. (7) and (11) for the *p*-type or Eqs. (6) and (12) for the *n*-type.

p-type:

$$[Y_i^{\cdots}] = \frac{K_F K_F^{A1.5}}{K_S^{0.5} K_{O_2}^{(O)0.5}} \times \exp\left[-\frac{\Delta G_F - \Delta G_S/2 + 3\Delta G_F^A/2 - \Delta H_{O_2}^{(O)}/2}{kT}\right] \tag{15}$$

n-type:

$$[Y_i^{\cdots}] = \frac{K_F K_{O_2}^{(R)0.5}}{K_S^{0.5}} \exp\left[-\frac{\Delta G_F - \Delta G_S/2 + \Delta H_{O_2}^{(R)}/2}{kT}\right] \tag{16}$$

From the conductivity data of Tallen and Vest,[25] we estimate $\Delta H_{O_2}^{(O)} = 5.82$ eV, and $\Delta H_{O_2}^{(R)} = 11.2$ eV. Furthermore, Odier

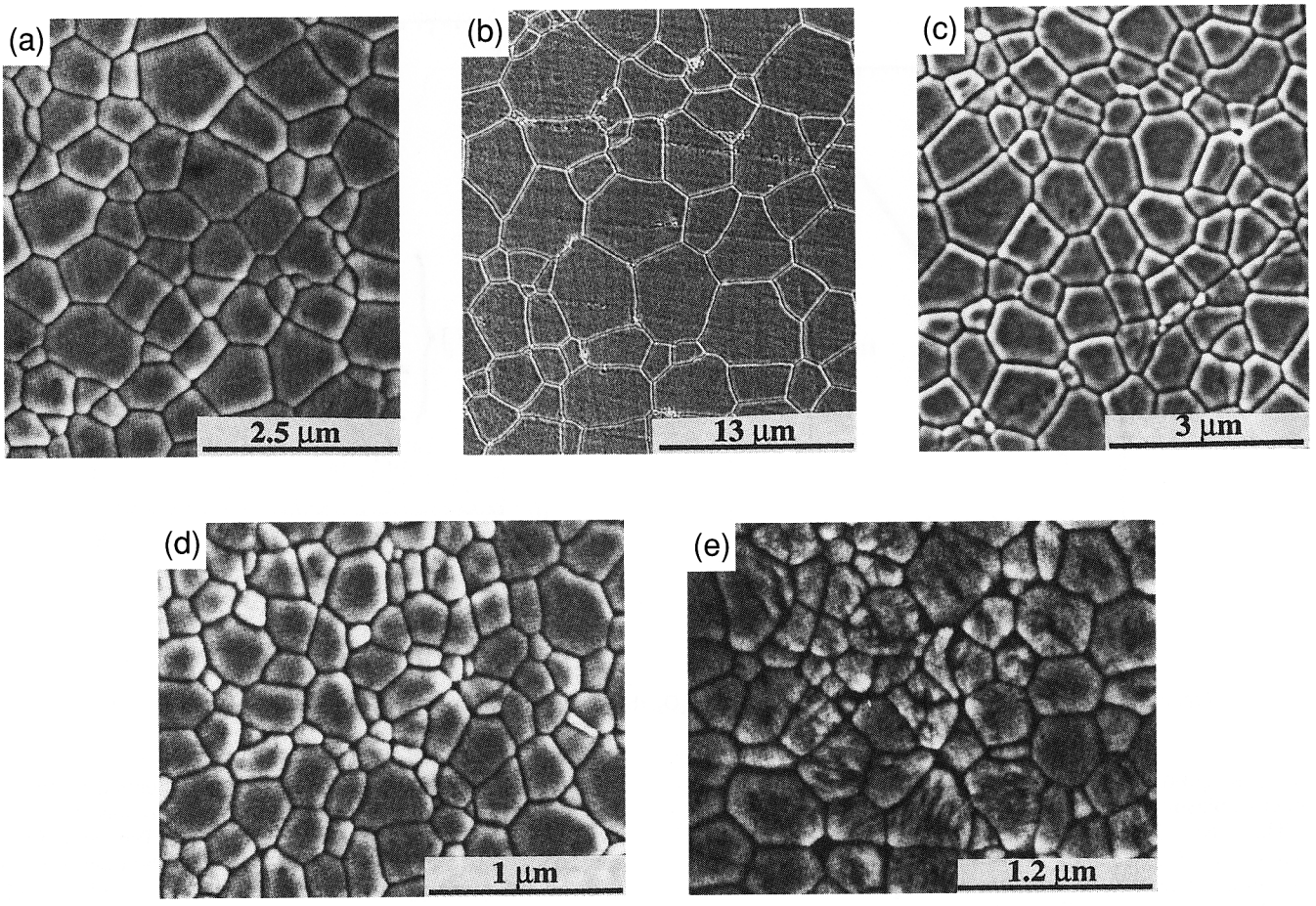

Fig. 3. Microstructures of undoped and doped Y_2O_3 sintered at 1500°C for 27 h: (a) Y_2O_3, (b) 1.0% Sr, (c) 1.0% Yb, (d) 1.0% Zr, (e) 1.0% Nb.

and Loup[28] reported that the thermal band gap is about 5.5 eV. These data allow us to obtain from Eqs. (3), (8), and (9), $\Delta G_F^A = 6.0$ eV. From consideration of the defect reaction

$$3V_O^{\cdot\cdot} + 2Y_Y \xrightarrow{2\Delta G_F - \Delta G_S} 2Y_i^{\cdot\cdot\cdot} \quad (17)$$

we believe the energy $\Delta G_F - \Delta G_S/2$ should be nonnegative since anion defects should be easier to move than cation defects in Y_2O_3. This then places an upper bound of the activation energy of $[Y_i^{\cdot\cdot\cdot}]$ at 6.1 eV in *p*-type and 5.6 eV in *n*-type. These values are higher than the measured activation energy of grain boundary mobility, 4.1 eV for *p*-type (in air) and 3.7 eV for *n*-type (in 2% H_2). The reason for the overestimation probably lies in the overestimate of ΔG_F^A in the previous work. For UO_2, a nonstoichiometric compound, this value is much lower, 3.0 eV.[29] Values around 6.0 eV are more typically associated with highly stoichiometric compounds such as BeO and MgO.[30] For Y_2O_3, which is more like a nonstoichiometric compound such as UO_2 than BeO or MgO, it seems that an estimate of ΔG_F^A around 4.5 eV is more reasonable. This gives an activation energy of 3.8 eV for the *p*-type. If we use the same ΔG_F^A to revise the estimate of $\Delta H_{O_2}^{(R)}$ to be 9.7 eV, we also arrive at an activation energy of 4.8 eV for the *n*-type. These estimates compare more reasonably with our data on grain boundary

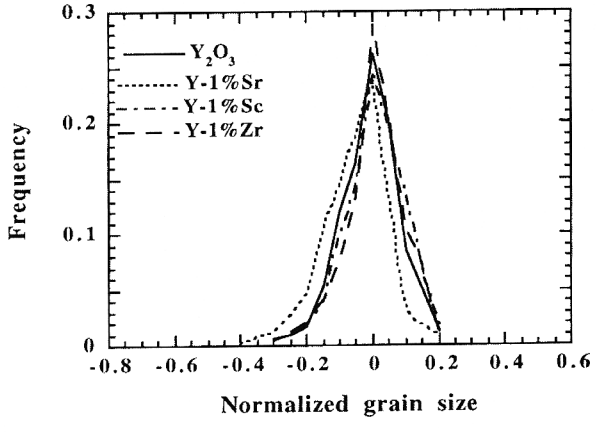

Fig. 4. Grain size distributions of undoped and doped Y_2O_3. Grain size is normalized by mean grain size in each case, which varies from 0.73 to 9.7 μm.

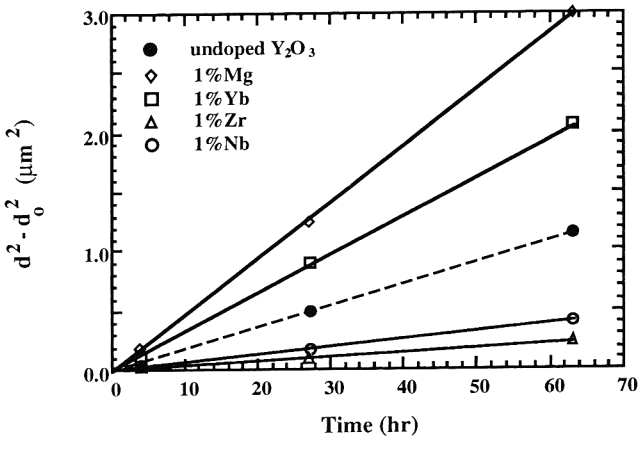

Fig. 5. Grain growth kinetics of Y_2O_3 at 1500°C; dopants as indicated.

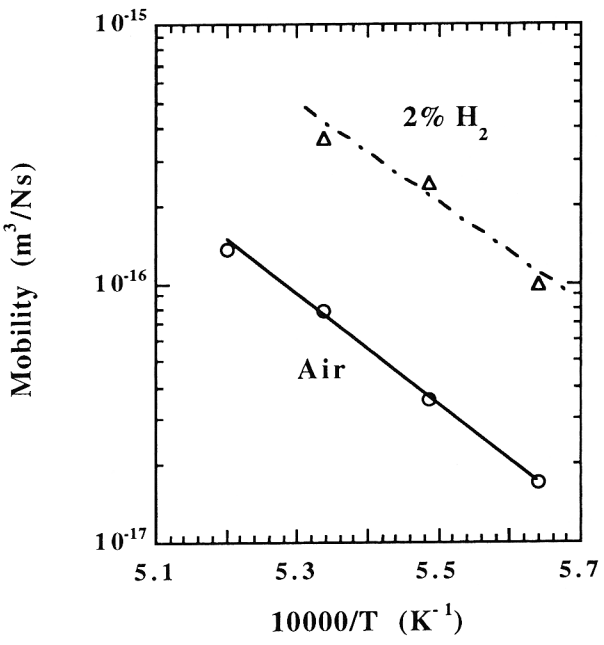

Fig. 6. Temperature dependence of grain boundary mobility of undoped Y_2O_3 sintered in air and 2% H_2.

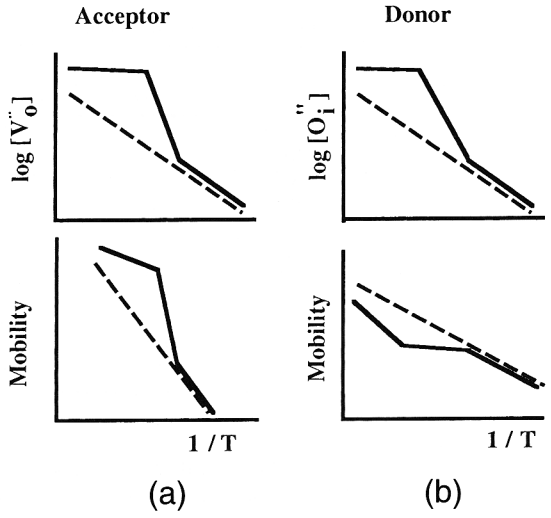

Fig. 8. Schematics for defect concentration and grain boundary mobility in (a) acceptor doping and (b) donor doping, with dashed lines representing the undoped Y_2O_3. At high temperatures, concentrations of $[V_O^{\cdot\cdot}]$ and $[O_i'']$ reach constant values dictated by the concentrations of acceptor and donor. At low temperatures, they approach the values of intrinsic defects in Y_2O_3. The mobility is schematically drawn with a shape similar to $[V_O^{\cdot\cdot}]^{1.5}$ or $[O_i'']^{-1.5}$ but with a higher slope due to other contributions to the activation energy.

mobility provided the activation energy for interstitial migration is nearly zero. (The same observation on migration energy was previously made for cation migration in the grain boundary in CeO_2.[1,2])

(2) *Acceptor and Donor Doping*

We now consider divalent and tetravalent dopants. We first compare the mobility data of undoped Y_2O_3 and those doped with Sr^{2+} and Zr^{4+}. These data are shown as solid lines in Fig. 7. We have also included dopants which either are much smaller (Mg^{2+} and Nb^{5+}) or have a tendency to reduce to lower valence states (Ti^{4+} and Ce^{4+}) and plot their data as dashed lines in Fig. 7. The solid lines in Fig. 7 show a clear trend of acceptor dopant enhancing grain boundary mobility, whereas donor dopants do the opposite. This trend is consistent with the cation interstitial mechanism.

The activation energy for acceptor doping is typically higher than that for undoped Y_2O_3, which is in turn higher than that for donor doping. (Ti doping is an exception; in this case, charge consideration is complicated by mixed valence states.) This has the consequence of making the enhancement/suppression effects of dopants more pronounced at higher temperatures than at lower temperatures. In the context of the interstitial mechanism, this implies a higher relative concentration of $[V_O^{\cdot\cdot}]$ (for acceptor doping) or $[O_i'']$ (for donor doping), compared with undoped Y_2O_3, as the temperature increases. A simple interpretation of this observation is that the extrinsic defects are bound to the dopants at lower temperatures, and become dissociated only at higher temperature, rendering the dopant effect on $[Y_i^{\cdot\cdot\cdot}]$ increasingly obvious. As schematically shown in Fig. 8, this can cause the mobility in the intermediate temperature range to take a different activation energy in a way that is consistent with our observation.

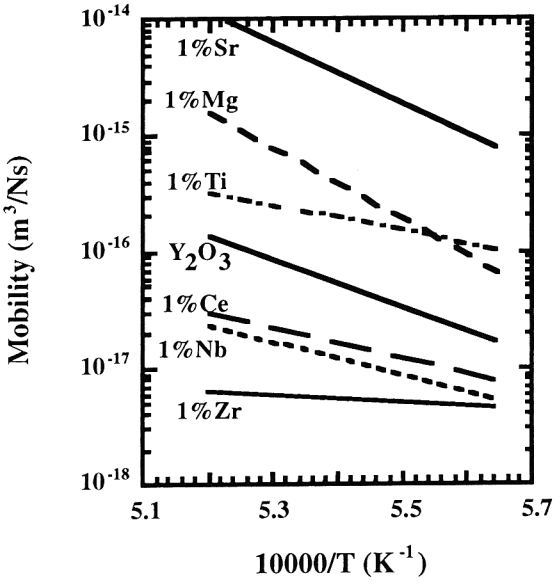

Fig. 7. Temperature dependence of grain boundary mobility; dopants as indicated.

Because of the lack of reliable data for various energies in Y_2O_3, an accurate estimate of the association energy between defects and dopants cannot be obtained at this time. For a rough estimate, though, we let $\Delta G_F - \Delta G_S/2 = 0$ (say $\Delta G_F = 5$ eV and $\Delta G_S = 10$ eV). Then, for acceptor doping, we expect Eq. (6) to apply. The contribution to the activation energy, except that for $V_O^{\cdot\cdot}$ and for interstitial migration, is $\Delta G_F - \Delta G_S/2$, which is zero. Thus, the very large activation energy of grain boundary mobility (5.3 eV for Sr doping) is mostly due to a very strong binding between $V_O^{\cdot\cdot}$ and acceptor dopants, of the order of 3.6 eV ($[Y_i^{\cdot\cdot\cdot}] \propto [V_O^{\cdot\cdot}]^{1.5}$). For donor doping, we expect Eq. (7) to hold. The contribution to the activation energy, except that for O_i'' and for interstitial migration, is $\Delta G_F - \Delta G_S/2 + 3\Delta G_F^A/2$, or 6.7 eV if $\Delta G_F - \Delta G_S/2$ is zero. Thus, the very small activation energy for grain boundary mobility (0.7 eV for Zr doping) is mostly due to a very strong binding energy between O_i'' and donor dopants, of the order of 4 eV ($[Y_i^{\cdot\cdot\cdot}] \propto [O_i'''']^{-1.5}$).

Other data of acceptor and donor doping can be rationalized by taking into account additional effects associated with dopant size and charges. Mg^{2+} doping is less effective than Sr^{2+} doping in enhancing mobility and it has a higher activation energy. This may be attributed to an even stronger binding between $V_O^{\cdot\cdot}$ and Mg, presumably due to the larger elastic distortion associated with the undersized dopant as discussed in our CeO_2 paper.[2] Ce^{4+} doping has a smaller suppression effect on mobility than Zr^{4+} doping, presumably because Ce^{4+} tends to reduce to Ce^{3+} at higher temperature, thus decreasing the net effect of

Table II. Grain Boundary Mobility of Undoped and 1.0%-Doped Y_2O_3 in Air

	Mobility ($\times 10^{-17}$ m^3/(N·s))				Activation energy (eV)
	1500°C	1550°C	1600°C	1650°C	
Y_2O_3	1.7	3.5	7.9	13.6	4.14
Mg^{2+}	6.4	20	70	159	6.80
Sr^{2+}	63	251	584	965	5.35
Sc^{3+}	2.8	7.3	18	38	5.1
Yb^{3+}	7.6	13	29	46	3.64
Gd^{3+}	9.2	16	31	54	3.51
La^{3+}	9.8	19	43	80	4.17
Ti^{4+}	9.3	16	23	30	2.28
Zr^{4+}	0.47	0.52	0.61	0.65	0.67
Ce^{4+}	0.78	1.1	1.8	2.8	2.54
Nb^{5+}	0.58	0.86	1.5	2.4	2.82

donor doping, and decreasing the activation energy somewhat. Nb^{5+}, in theory, should be a more potent donor than Zr^{4+}. However, this charge effect is countered by the much smaller size of Nb^{5+}, which probably distorts the lattice severely and facilitates defect migration as discussed in the previous paper,[2] resulting in a somewhat smaller suppression effect than Zr^{4+}. Lastly, Ti^{4+} is both severely undersized and amenable to charge reduction. Thus, unlike Zr^{4+}, Ti^{4+} doping is anomalous and actually increases the grain boundary mobility to some extent.

An attempt to further model the defect concentration and to fit the observed mobility data in Sr- and Zr-doped materials is described in the Appendix, which essentially confirms the above qualitative discussion as outlined in Fig. 8.

(3) Trivalent Dopants

Doping by trivalent dopants, in principle, should not affect defect population and thus has no effect on grain boundary mobility. Trivalent dopants, however, generally increase the grain boundary mobility somewhat, by a factor of 2–5 times, but the enhancement effect is much smaller than that caused by acceptor dopants. This is shown in Fig. 9, which includes all the trivalent dopant data along with those of undoped Y_2O_3. Since the activation energy of these doped Y_2O_3 is generally comparable to that of undoped Y_2O_3, around 4 eV, it suggests the same grain boundary diffusion mechanism. The modestly enhanced mobility may be due to a slight distortion of the lattice or a slight modulation of the phonon vibration spectra that leads to a slightly higher migration rate for the cation interstitial and hence a modestly higher mobility. Alternatively, it may also be due to the disordering effect of solid solution that could perturb the ordering of unoccupied anion sites in Fig. 1, although the exact cause of these dopant effects cannot be ascertained at this time.

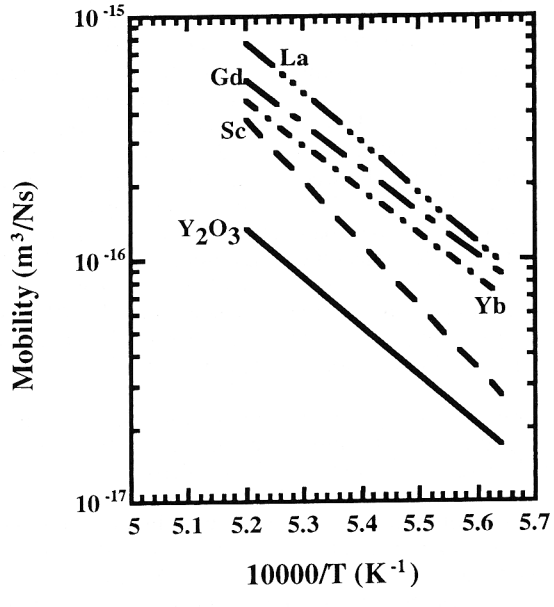

Fig. 9. Effect of 1.0% trivalent dopants on the grain boundary mobility in Y_2O_3.

VI. Discussion

(1) Grain Boundary Mobility

Kinetic studies on the dopant effects on Y_2O_3 have been reported by various authors.[12,31–34] These results are summarized in Table III. Overall, these results are consistent with our findings in that divalent and trivalent dopants enhance kinetics and tetravalent dopants suppress kinetics. For example, Th should behave similarly to Zr, Ca similarly to Mg, and both La and Sr have also been investigated in our work. Although different interpretations have been proposed by the investigators of these studies, they were based on the result of a single dopant and lacked the broad basis of the present study. Taken together, we believe our interpretation based on the cation interstitial mechanism is consistent with all the known data on the dopant effect.

Comparing the dopant effects on Y_2O_3 and CeO_2, we note that solute drag on grain boundaries was clearly demonstrated in CeO_2,[2] but we were not able to do so in Y_2O_3. Solute drag is due to segregation over a distance beyond the grain boundary thickness. Since dragging the solute along with a migrating grain boundary entails lattice diffusion ($\mathcal{D}_L$), which is presumably more sluggish than grain boundary diffusion, the effective mobility of the grain boundary is lower than that caused by grain boundary diffusion alone. Thus, the addition of solute is predicted to lower the grain boundary mobility if solute segregation occurs over a relatively long distance from the grain boundary. Although the above prediction has been generally accepted, it is based on the assumption that neither grain boundary nor lattice diffusivity is influenced by the dopant. While this assumption may be acceptable for metals, it is generally incorrect for ceramics. Accepting the possibility that solute may modify the diffusivity, we can schematically illustrate the net solute effect in Fig. 10. At low concentration, grain boundary mobility is controlled by grain boundary diffusivity $\mathcal{D}_B$. Thus, the normalized mobility, defined as (mobility of doped solid)/(mobility of undoped solid), increases or decreases depending on whether the solute enhances or suppresses diffusion. At high concentration, solute drag becomes predominant and the grain boundary mobility is controlled by lattice diffusion. This results in a relative decrease in the normalized mobility although, for diffusion-enhancing solute, the suppression effect may not appear strong enough unless $\mathcal{D}_B \gg \mathcal{D}_L$. Moreover, as the concentration further increases, the diffusion enhancement may again overtake the solute drag effect. It is also clear that, for diffusion-suppressing solutes, it would be difficult to definitively establish the solute drag effect, given that the normalized mobility monotonically decreases with solute concentration anyway. Thus, to demonstrate the solute drag effect, we need

Table III. Summary of the Dopant Effect on the Kinetics of Y_2O_3 in the Literature

Dopant	Concentration (% MO_x)	Method	Observation kinetics	Ref.
Th	1–11	Grain growth	Suppressed	31
Th	10	Sintering	Suppressed	32
La	≤6.7	Grain growth	Enhanced	33
Sr	0.3–1.2	Sintering	Enhanced	12
Ca	0–10	Sintering	Enhanced	34

to study diffusion-enhancing solutes in materials that have $\mathcal{D}_B \gg \mathcal{D}_L$.

Selected data of grain boundary mobility of Y_2O_3 and CeO_2 systems are plotted in Fig. 11 to outline the broad range of mobility values in these materials. It is clear that Y_2O_3 has generally lower mobility than CeO_2 at the same temperature. This is not due to a different homologous temperature, since Y_2O_3 actually has a slightly lower melting point (2410°C) than CeO_2 (2600°C). Indeed, comparing Y_2O_3 with other fluorite-structure oxides, such as tetragonal ZrO_2 and cubic ZrO_2,[35] also shown in Fig. 11, we find Y_2O_3 has a much lower grain boundary mobility than these oxides. (The melting point of ZrO_2 is 2700°C.) This may indicate that the grain boundary diffusivities of doped and undoped Y_2O_3 are relatively low and are already close in magnitude to those of lattice diffusivity. Thus, according to Fig. 10, this would cause some difficulty in demonstrating the solute drag effect. Although further studies of the concentration effect may prove insightful, they are unfortunately limited by the relatively low solubility of both of the diffusion-enhancing dopants, Mg and Sr, investigated here (see Table I).

(2) Defect Chemistry

A further comparison of the defect chemistry in Y_2O_3 and fluorite-structure MO_2 can be made on the much larger interaction energy between aliovalent dopant and anion defects in Y_2O_3 and on the difference in Nb solubility. Regarding the former, we note that according to our study, a binding energy of the order of 3–4 eV exists between aliovalent dopants and anion defects. This contrasts with a much smaller, by 1 order of magnitude, binding energy in CeO_2 which has been consistently inferred by the data of ionic conductivity[36–38] and grain boundary mobility.[2] A crude estimate of the Coulombic binding energy can be made in the form (in cgs units) of $4e^2/\varepsilon r$, where e is elementary charge, ε is the dielectric constant, and r is the nearest distance between cation dopant and anion defects. In the above, the factor 4 in the numerator arises from the effective charge of anion defects and the fact that two aliovalent cations (Sr^{2+} or Zr^{4+}, for example) are likely to cluster around one anion defect. Using $\varepsilon = 4.64$ and $r = 2.2$ Å (for V_O) to 2.5 Å (for O_i),[39,40] an estimate from 4.95 to 5.63 eV is obtained. In CeO_2, such Coulombic energy contribution is largely lowered due to elastic and dielectric relaxation of the matrix.[41] In Y_2O_3, however, recent preliminary lattice static calculation using the Mott–Littleson model seems to at least partially validate the large magnitude of the above estimate.[42] This suggests a much more ionic matrix in Y_2O_3 which does not relax to the same extent as in CeO_2.

We note that in both CeO_2 and ZrO_2, the solubility of Nb^{5+} is very limited, indicating difficulty in generating O_i. This is in contrast with the large Nb^{5+} solubility in Y_2O_3 (see Table I). Thus, it seems that both V_O and O_i are equally likely to form in Y_2O_3, whereas CeO_2 and ZrO_2 strongly favor V_O over O_i. (The above conclusion is reasonable in view of the different crystal structures of Y_2O_3 and fluorite structured oxides, especially the existence of missing oxygens in the former as shown in Fig. 1.) This could also imply that at grain boundaries, where defect equilibrium is presumably maintained, the relative population of V_O and O_i would be similar in Y_2O_3 but would be richer in V_O in CeO_2 and ZrO_2. If so, we may further speculate on a more stoichiometric composition at the grain boundary in Y_2O_3 compared to CeO_2 and ZrO_2, which, in turn, could cause a lower grain boundary diffusivity in Y_2O_3.

VII. Conclusions

(1) In Y_2O_3, grain boundary mobility is controlled by cation diffusivity, and cations diffuse by an interstitial mechanism that can be enhanced by the presence of oxygen vacancies and suppressed by the presence of oxygen interstitials.

(2) Acceptor dopants, which introduce oxygen vacancies, enhance the grain boundary mobility. Donor dopants, which introduce oxygen interstitials, suppress the grain boundary mobility. Overall, Sr^{2+} increases grain boundary mobility the most and Zr^{4+} decreases grain boundary mobility the most.

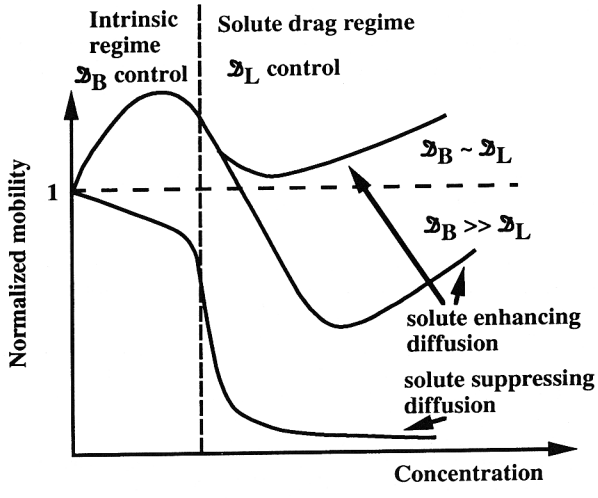

Fig. 10. Schematic for solute effect on grain boundary mobility.

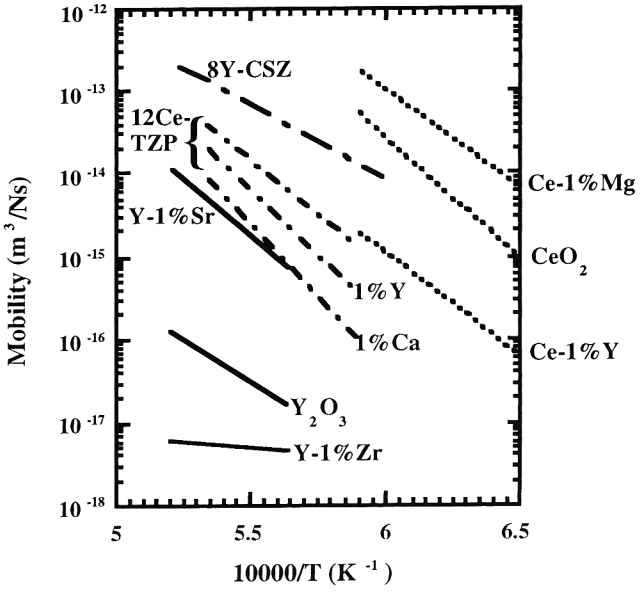

Fig. 11. Grain boundary mobility of CeO_2, Y_2O_3, and ZrO_2 systems.

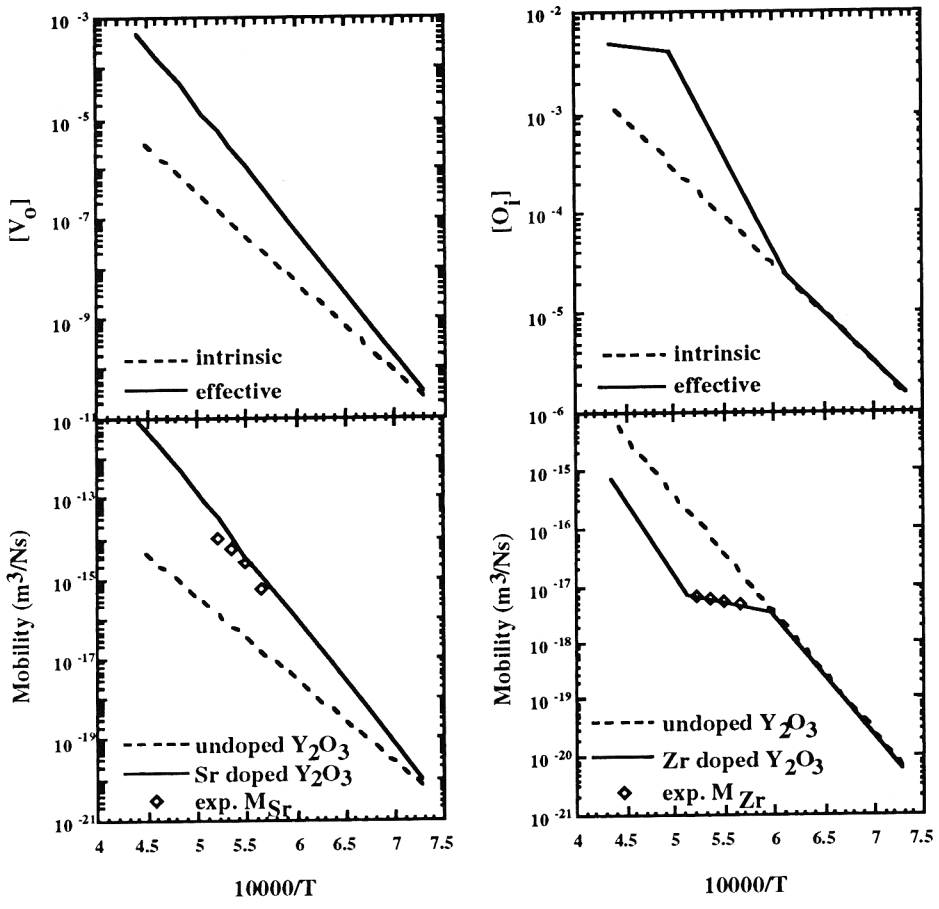

Fig. A1. Calculated oxygen defect concentrations and grain boundary mobilities in both acceptor- and donor-doped Y_2O_3.

(3) The anomalous effect of undersized dopants (Ti and Nb) on enhancing grain boundary mobility cannot be explained in terms of valence alone, but is likely due to lattice distortion, which is consistent with similar findings in CeO_2.

(4) Activation energies of grain boundary mobility vary from 0.67 eV (Zr doping) to 6.8 eV (Mg doping), indicating a very strong binding energy between dopants and oxygen defects.

(5) Cation migration via an interstitial mechanism is suggested to be a general mechanism that dominates diffusive processes in fluorite and modified fluorite-structured oxides such as CeO_2, UO_2, ZrO_2, Y_2O_3, and cubic Bi_2O_3.

APPENDIX

Defect Concentration and Grain Boundary Mobility

The concentration of effective oxygen vacancy as a function of temperature in the presence of acceptor dopant is calculated by the following equation:

$$[V_O]_{eff} = \frac{\frac{1}{2}[D_a]}{1 + A_a \exp(B_a/kT)} \quad \text{(A-1)}$$

where $[D_a]$ is the concentration of acceptor dopant, A_a is 6.76×10^{-11}, B_a is the binding energy between acceptor dopant and oxygen vacancy, which is 5 eV, and kT has its usual meaning. Further, the grain boundary mobility of Y_2O_3 with acceptor dopant can be obtained by

$$M_a = \left(\frac{[V_O]_{eff}}{[V_O]_{intrinsic}}\right)^{1.5} M_Y \quad \text{(A-2)}$$

where $[V_O]_{intrinsic}$ is the concentration of intrinsic oxygen vacancy, and M_Y is the grain boundary mobility of undoped Y_2O_3.

Similarly, the concentration of effective oxygen interstitial and the grain boundary mobility of Y_2O_3 doped with donor dopant can be obtained from the following equations:

$$[O_i]_{eff} = \frac{\frac{1}{2}[D_d]}{1 + A_d \exp(B_d/kT)} \quad \text{(A-3)}$$

$$M_d = \left(\frac{[O_i]_{intrinsic}}{[O_i]_{eff}}\right)^{1.5} M_Y \quad \text{(A-4)}$$

where $[D_d]$ is the concentration of donor dopant, A_d is 1.833×10^{-13}, B_d is the binding energy between donor dopant and oxygen interstitial, which is 5 eV, $[O_i]_{intrinsic}$ is the concentration of intrinsic oxygen interstitial, and M_d is the grain boundary mobility of Y_2O_3 doped with donor dopant. As shown in Fig. A1, the grain boundary mobility of Y_2O_3 doped with either acceptor or donor dopant can be shown to agree with the above calculation.

References

[1]P.-L. Chen and I-W. Chen, "The Role of Defect Interaction in Boundary Mobility and Cation Diffusivity of CeO_2," *J. Am. Ceram. Soc.*, **77** [9] 2289–97 (1994).

[2]P.-L. Chen and I-W. Chen, "Grain Growth in CeO_2: Dopant Effects, Defect Mechanism, and Solute Drag," *J. Am. Ceram. Soc.*, **79** [7] 1793–800 (1996).

[3]H. Matzke, "Lattice Disorder and Metal Self-Diffusion in Nonstoichiometric UO_2 and $(U,Pu)O_2$," *J. Phys. (Paris) Suppl.*, **34** [11–12] C9-317–25 (1973).

[4]M. H. Rand and T. L. Markin, "Some Thermodynamic Aspects of $(U,Pu)O_2$ Solid Solutions and Their Use as Nuclear Fuels"; pp. 637–50 in *Thermodynamics of Nuclear Materials*. International Atomic Energy Agency, Vienna, 1967.

[5]B. Burton, "Prediction of Creep Behavior from Diffusion Data in UO_2 Nuclear Fuel"; pp. 415–35 in *Thermodynamics of Nuclear Materials*, Vol. I. International Atomic Energy Agency, Vienna, 1967.

[6]J. L. Routbort, N. A. Jared, and J. C. Voglewede, "Compression Creep of Mixed-Oxide Fuel Pellets," *J. Nucl. Mater.*, **44**, 247–59 (1972).

[7]J. R. MacEuan and J. Hayashi, "Grain Growth in UO_2 III. Some Factors Influencing Equiaxed Grain Growth," *Proc. Br. Ceram. Soc.*, **6**, 245–72 (1967).

[8]T. Norby and P. Kofstad, "Electrical Conductivity and Defect Structure of Y_2O_3 as a Function of Water Vapor Pressure," *J. Am. Ceram. Soc.*, **67** [12] 786–92 (1984).

[9]T. Norby and P. Kofstad, "Direct-Current Conductivity of Y_2O_3 as a Function of Water Vapor Pressure," *J. Am. Ceram. Soc.*, **69** [11] 780–83 (1986).

[10]T. Norby and P. Kofstad, "Electrical Conductivity of Y_2O_3 as a Function of Oxygen Partial Pressure in Wet and Dry Atmospheres," *J. Am. Ceram. Soc.*, **69** [11] 784–89 (1986).

[11]T. Norby and P. Kofstad, "Proton and Native-Ion Conductivities in Y_2O_3 at High Temperatures," *Solid State Ionics*, **20**, 169–84 (1986).

[12]C. Greskovich and C. R. O'clair, "Transparent, Sintered $Y_{2-x}Sr_xO_{3-1/2x}$," *Adv. Ceram. Mater.*, **1** [4] 350–55 (1986).

[13]E. C. Subbarao, P. H. Sutter, and J. Hrizo, "Defect Structure and Electrical Conductivity of ThO_2–Y_2O_3 Solid Solution," *J. Am. Ceram. Soc.*, **48** [9] 443–46 (1965).

[14]W. W. Barker and A. F. Wilson, "Gross Non-stoichiometry and Vacancy Ordering in the System Cerium Dioxide Yttrium Sesquioxide," *J. Inorg. Nucl. Chem.*, **30**, 1415–23 (1968).

[15]K. Ando, Y. Oishi, and H. Hase, "Oxygen Self-Diffusion in Single-Crystal Y_2O_3," *J. Am. Ceram. Soc.*, **66** [12] C-222–C-223 (1983).

[16]M. F. Berard and D. R. Wilder, "Cation Self-Diffusion in Polycrystalline Y_2O_3 and Er_2O_3," *J. Am. Ceram. Soc.*, **52** [2] 85–88 (1969).

[17]R. D. Shannon, "Revised Effective Ionic Radii and Systematic Studies of Interatomic Distances, Halides and Chalcogenides," *Acta Crystallogr.*, **A32**, 756 (1976).

[18]S. G. Tresvyatskii, L. M. Lopato, A. A. Ogorodnikova, and A. V. Shevchenko, "Phase Diagrams of the Systems Formed by Yttrium, Erbium, and Ytterbium Oxides with Magnesium Oxide," *Inorg. Mater.*, **7** [11] 1798–801 (1971).

[19]S. G. Tresvyatskii, L. M. Lopato, A. E. Kushchevskii, and A. V. Shevchenko, "Phase Diagrams of the Systems Y_2O_3–SrO and Yb_2O_3," *Inorg. Mater.*, **7** [10] 1614–17 (1971).

[20]E. M. Levin, H. F. McMurdie, and F. P. Hall, *Phase Diagrams for Ceramists*, Vol. I. American Ceramic Society, Columbus, OH, 1956.

[21]R. S. Roth (Ed.), *Phase Equilibrium Diagrams*, Vol. XI. American Ceramic Society, Westerville, OH, 1995.

[22]J. Coutures and M. Foex, "High Temperature Equilibria in the System La_2O_3–Y_2O_3," *J. Solid State Chem.*, **11** [4] 294–300 (1974).

[23]P. Duwes, F. H. Brown, and F. Odell, "The Zirconia–Yttria System," *J. Electrochem. Soc.*, **98** [9] 356–62 (1951).

[24]T. Ishihara, K. Sato, Y. Mizuhara, and Y. Takita, "Oxygen Ion Conductivity of Yttria–Niobia Mixed Oxide with Fluorite-Related Structure," *Solid State Ionics*, **50**, 227–31 (1992).

[25]N. M. Tallan and R. W. Vest, "Electrical Properties and Defect Structure of Y_2O_3," *J. Am. Ceram. Soc.*, **49** [9] 401–404 (1966).

[26]D. Sordelet and M. Akinc, "Preparation of Spherical, Monosized Y_2O_3 Precursor Particles," *J. Colloid Interface Sci.*, **122** [1] 47–59 (1988).

[27]R. L. Fullman, "Measurement of Particle Size in Opaque Bodies," *Trans. AIME*, **1970** [3] 447–52 (1953).

[28]P. Odier and J.-P. Loup, "An Unusual Technique for the Study of Nonstoichiometry: The Thermal Emission of Electrons Results for Y_2O_3 and TiO_2," *J. Solid State Chem.*, **34**, 107–19 (1980).

[29]H. Matzke, "The Effect of TiO_2 Additions on Defect Structure, Sintering and Gas Release of UO_2," AECL-2585, Atomic Energy of Canada Ltd., Chalk River, Ontario, Canada, 1966.

[30]W. D. Kingery, H. K. Bowen, and D. R. Uhlmann, *Introduction to Ceramics*. Wiley, New York, 1976.

[31]P. J. Jorgensen and R. C. Anderson, "Grain-Boundary Segregation and Final-Stage Sintering of Y_2O_3," *J. Am. Ceram. Soc.*, **50** [11] 553–58 (1967).

[32]C. Greskovich and K. N. Woods, "Fabrication of Transparent ThO_2-Doped Y_2O_3," *Am. Ceram. Soc. Bull.*, **52** [5] 473–78 (1973).

[33]W. H. Rhodes, "Controlled Transient Solid Second-Phase Sintering of Yttria," *J. Am. Ceram. Soc.*, **64** [1] 13–19 (1981).

[34]K. Katayama, H. Osawa, T. Akiba, and H. Yanagida, "Sintering and Electrical Properties of CaO-Doped Y_2O_3," *J. Eur. Ceram. Soc.*, **6**, 39–45 (1990).

[35]S. L. Hwang and I-W. Chen, "Grain Size Control of Tetragonal Zirconia Polycrystals Using the Space Charge Concept," *J. Am. Ceram. Soc.*, **73** [11] 3269–77 (1990).

[36]A. S. Nowick, D. Y. Wang, D. S. Park, and J. Griffith, "Oxygen-Ion Conductivity and Defect Structure of CeO_2"; pp. 673–81 in *Fast Ion Transport in Solids*. Edited by P. Vashishta, J. N. Mundy, and G. K. Shenoy. Elsevier North Holland, Amsterdam, Netherlands, 1979.

[37]R. Gerhardt-Anderson and A. S. Nowick, "Ionic Conductivity of CeO_2 with Trivalent Dopants of Different Ionic Radii," *Solid State Ionics*, **5**, 547–50 (1981).

[38]D. Y. Wang and A. S. Nowick, "Dielectric Relaxation from a Network of Charged Defects in Dilute CeO_2:Y_2O_3 Solid Solutions," *Solid State Ionics*, **5**, 551–54 (1981).

[39]W. Y. Ching; private communication.

[40]W. Y. Ching and Y. N. Xu, "Electronic and Optical Properties of Yttria," *Phys. Rev. Lett.*, **65** [7] 895–98 (1990).

[41]V. Butler, C. R. A. Catlow, B. E. F. Fender, and J. H. Harding, "Dopant Ion Radius and Ionic Conductivity in Cerium Dioxide," *Solid State Ionics*, **8**, 109–13 (1983).

[42]R. W. Grimes; private communication. □